Observation of Chiral Symmetry Breaking in Toroidal Vortices of Light

Wei Chen,[1,*] Yuan Liu,[1,*] An-Zhuo Yu,[1] Han Cao,[1] Wei Hu,[1] Wen Qiao,[2,3,†] Lin-Sen Chen,[2,3,‡] and Yan-Qing Lu[1,§]

[1]National Laboratory of Solid State Microstructures, Key Laboratory of Intelligent Optical Sensing and Manipulation, College of Engineering and Applied Sciences, and Collaborative Innovation Center of Advanced Microstructures, Nanjing University, Nanjing 210093, China

[2]School of Optoelectronic Science and Engineering and Collaborative Innovation Center of Suzhou Nano Science and Technology, Soochow University, 215006 Suzhou, China

[3]Key Lab of Advanced Optical Manufacturing Technologies of Jiangsu Province and Key Lab of Modern Optical Technologies of Education Ministry of China, Soochow University, 215006 Suzhou, China

(Received 11 April 2023; accepted 4 March 2024; published 12 April 2024)

In this Letter, we explore the intersection of chirality and recently discovered toroidal spatiotemporal optical vortices (STOVs). We introduce "photonic conchs" theoretically as a new type of toroidal-like state exhibiting geometrical chirality, and experimentally observe these wave packets with controllable topological charges. Unlike toroidal STOVs, photonic conchs exhibit unique chirality-related dynamical evolution in free space and possess an orbital angular momentum correlated with all the dimensions of space-time. This research deepens our understanding of toroidal light states and potentially advances various fields by unveiling similar wave phenomena in a broader scope of physics systems, including acoustics and electronics.

DOI: 10.1103/PhysRevLett.132.153801

Introduction.—Chirality is widespread in nature and science [1–7], representing broken symmetry where an object cannot superimpose onto its mirror image via simple translation or rotation. Chirality has also been observed in various toroidal systems [8–11], wherein toroidal vortices emerge as particularly fascinating symmetrical structures [8–14]. Recently, two optical toroidal vortices have attracted considerable attention [15,16]. One is the toroidal light pulse (TLP) [17], visualized as a torus of electric (or magnetic) field lines [Fig. 1(a)]; however, realizing single-cycle TLPs in the optical domain remains challenging [15]. Another comes from a spatiotemporal optical vortex (STOV) [18–27] with its transverse orbital angular momentum (OAM) vector bent into a ring [16] [Fig. 1(b)]. This ringlike structure—exhibiting a twisting helical phase around the closed circle—can be quantified by a topological charge [16].

However, although toroidal STOVs can be theoretically derived under anomalous dispersion, their behavior in vacuum and normal dispersion remains mysterious [16]. Experimentally observing higher-order toroidal STOVs also poses difficulties. Furthermore, the angle-invariant distribution of toroidal STOVs suggests no additional exploitable dimension compared to conventional STOVs, restricting their applications. Here, we investigate chiral symmetry breaking in toroidal STOVs. Using inverse spiral transformation [28] to solve the forward Maxwell equation (FME) [29,30], we obtain toroidal-like solutions possessing geometrical chirality determined by the signs of their characteristic spiral parameters and topological charges. These "photonic conchs" with adjustable topological charges can be generated experimentally and exhibit chirality-related dynamical evolution. We attribute such dynamics to quantifiable azimuthal intrinsic dispersion and

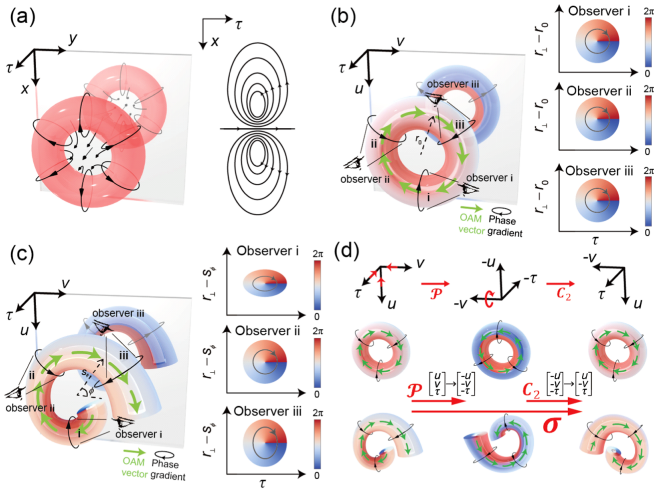

FIG. 1. (a) TLP. (b) Toroidal STOV. (c) Photonic conch. Insets in (b),(c) show the local field phase (observed by three "observers") in three radial-temporal planes marked by black circular arrows on the left. (d) Symmetry analysis for toroidal STOV and photonic conch.

confirm the resulting space-time varying OAM, indicating that chirality provides a new dimension for tailoring toroidal states.

Theoretical photonic conch.—We first briefly review the toroidal STOV investigated by Wan *et al.* [16], who obtained a spatiotemporal Laguerre-Gauss wave packet (one type of STOV) $\hat{\psi}(\hat{r},\hat{\varphi},\xi=0)=(\sqrt{2}\hat{r}/\hat{w}_0)^{|\ell|}L_m^{|\ell|}(2\hat{r}^2/\hat{w}_0^2)\exp[-(\hat{r}^2/\hat{w}_0^2)]\exp(-i\ell\hat{\varphi})$ satisfying the dimensionless wave equation in anomalous dispersion [31] $\partial^2\hat{\psi}/\partial\hat{r}^2+(1/\hat{r})(\partial\hat{\psi}/\partial\hat{r})+(1/\hat{r}^2)(\partial^2\hat{\psi}/\partial\hat{\varphi}^2)+2i\partial\hat{\psi}/\partial\xi=0$. Here, $L_m^{|\ell|}$ is the Laguerre polynomial, m and ℓ the radial and angular mode numbers, $\hat{r}=\sqrt{\hat{x}^2+\hat{\tau}^2}$ and $\hat{\varphi}=\mathrm{atan}(\hat{x}/\hat{\tau})$ the polar coordinates in the $\hat{x}-\hat{\tau}$ plane, ξ the normalized propagation distance, and $\hat{w}_0$ the beam waist. Note that "$\hat{}$" means dimensionless coordinates defined by $\hat{x}=x/x_s$ and $\hat{\tau}=t/t_s$, where x_s and t_s are the spatiotemporal widths of the wave packet [16]. Then, by adopting log-polar-to-Cartesian transformation [32] that satisfies $\hat{u}=\hat{r}_0\exp(-\hat{x}/\hat{b})\cos(\hat{y}/\hat{b})$ and $\hat{v}=\hat{r}_0\exp(-\hat{x}/\hat{b})\sin(\hat{y}/\hat{b})$ (parameter $\hat{b}$ translates a $2\pi\hat{b}$ length line to a closed circle; $\hat{r}_0$ is independent of $\hat{b}$ and determines the circle's radius), they obtained a toroidal solution in the $\hat{u}-\hat{v}$ plane [16] ($\xi=0$):

$$\hat{\psi}=\left[\frac{\sqrt{(\hat{r}_\perp-\hat{r}_0)^2+\hat{\tau}^2}}{\sqrt{\hat{z}_0}}\right]^{|\ell|}\exp\left[-\frac{(\hat{r}_\perp-\hat{r}_0)^2+\hat{\tau}^2}{2\hat{z}_0}\right]\times\exp\left[-i\ell\,\mathrm{atan}\left(\frac{\hat{\tau}}{\hat{r}_\perp-\hat{r}_0}\right)\right]. \tag{1}$$

Here, $\hat{r}_\perp=\sqrt{\hat{u}^2+\hat{v}^2}$, $\hat{z}_0$ is a constant, and $\hat{r}_0$ is the radius of the toroidal STOV [Fig. 1(b)].

Next, we turn to the photonic conch, beginning with the FME written in the form of envelope equations without nonlinear terms [29,30] $\partial\psi/\partial z=-(i\beta_2/2)(\partial^2\psi/\partial\tau^2)+(i/2\beta_0)(\partial^2/\partial x^2+\partial^2/\partial y^2)\psi$, where ψ is the complex envelope of electric field, $\tau=t-z/v_g$ the local time in a pulse frame (v_g is the group velocity), $\beta_n=d^nk(\omega)/d\omega^n|_{\omega=\omega_0}$ the medium dispersion [$k(\omega)$ and ω_0 are the wave number and central angular frequency]. Note that x, y, and τ are dimensional coordinates. Spatiotemporal Bessel (STB) vortex tubes (another type of STOV) along the y axis represent a solution to FME under anomalous dispersion ($\beta_2<0$):

$$\psi_{\ell_s}=(i)^{\ell_s}J_{\ell_s}\left[\sqrt{2\alpha\beta_0}\sqrt{x^2-\frac{\tau^2}{\beta_0\beta_2}}\right]\times\exp\left[i\ell_s\,\mathrm{atan}\left(\frac{x\sqrt{-\beta_0\beta_2}}{\tau}\right)\right]\exp(i\alpha z), \tag{2}$$

where α is a constant, and J_{ℓ_s} the ℓ_s-order Bessel function of the first kind (see detail in Supplemental Material [33]). We concentrate on STB vortices, given their experimental synthesizability with higher topological charges ℓ_s [27]. Conversely, the spatiotemporal Laguerre-Gauss vortices generated in recent experiments were limited to lower topological charges, e.g., $\ell_s=1$ and 2 [20–23].

Photonic conchs can be obtained by introducing inverse spiral transformation [28] to STB tubes. Such transformation maps a line to a spiral with $u=r_0\exp(ay/b+x/b)\cos(y/b-ax/b)$ and $v=r_0\exp(ay/b+x/b)\sin(y/b-ax/b)$. Here, b translates a $2\pi b$ length line to a spiral that exactly wraps around 2π, r_0 determines the azimuthal radius of the spiral, and a is the characteristic spiral parameter, whose sign determines the direction of the spiral curve (see detail in Supplemental Material [33]). The azimuthal angle ϕ in the remapped $u-v$ plane reads

$$\begin{aligned}\phi&=\phi_0+2m\pi\\ \phi_0&=\mathrm{atan}\left(\frac{v}{u}\right)\in[-\pi,\pi)\\ m&=\left\lfloor\frac{1}{2\pi a}\ln\left[\frac{r_\perp}{r_0}\exp(-a\phi_0)\right]\right\rfloor,\end{aligned} \tag{3}$$

where $r_\perp=\sqrt{u^2+v^2}$, and the operator $\lfloor\,\rfloor$ denotes the integer part. The photonic conch can be approximately expressed as ($z=0$):

$$E_{\ell_p}=(i)^{\ell_p}J_{\ell_p}\left[\sqrt{2\alpha\beta_0}\sqrt{(r_\perp-S_\phi)-\frac{\tau^2}{\beta_0\beta_2}}\right]\times\exp\left\{i\ell_p\,\mathrm{atan}\left[\frac{(r_\perp-S_\phi)\sqrt{-\beta_0\beta_2}}{\tau}\right]\right\}. \tag{4}$$

Here, $S_\phi=r_0\exp(a\phi)$ is the previously mentioned azimuthal radius, and ℓ_p is the topological charge, whose sign depends on the local field phase in each radial-temporal plane $(r_\perp-S_\phi,\tau)$ observed clockwise in the $u-v$ plane [see three "observers" in Fig. 1(c)]. For $a=0$, Eq. (4) reduces to a form similar to the toroidal STOV; otherwise, the field appears conchlike.

Although introducing the $u-v-\tau$ space facilitates understanding the conformal mapping, photonic conchs represent three-dimensional wave packets existing in real space, inherently introducing temporal modulation compared to conventional structured lights [41]. To verify the geometrical chirality, we apply a parity operation $\mathcal{P}$ $(u,v,\tau\to-u,-v,-\tau)$ to the photonic conch [Fig. 1(d)]. Since τ presents the pulse local time within a pulse frame, the relative velocity of the photonic conch to the τ axis during the $\tau\to-\tau$ operation is always zero. Combining with Eq. (3), the first term in Eq. (4) describing the field amplitude remains (rotated by π), while the second representing the phase gradient reverses.

According to chirality's definition, we further apply a twofold rotation operation $\boldsymbol{C}_2$ along the $-v/-u/-\tau$ axis

(where "/" means "or"), and the resulting structure still cannot overlap with the original [see the case of $\boldsymbol{C}_2$ along the $-v$ axis in Fig. 1(d)]. The combination of $\boldsymbol{\mathcal{P}}$ and $\boldsymbol{C}_2$ along the $-v/-u/-\tau$ axis is equivalent to a mirror reflection $\boldsymbol{\sigma}_{u\tau}/\boldsymbol{\sigma}_{v\tau}/\boldsymbol{\sigma}_{uv}$ vertical to the $-v/-u/-\tau$ axis, confirming the geometrical chirality of photonic conchs. Notably, the superposition of two beams—pre and postoperations $\boldsymbol{\sigma}_{u\tau}/\boldsymbol{\sigma}_{v\tau}$ and $\boldsymbol{\sigma}_{uv}$—can be respectively realized by modifying the signs of a and ℓ_p, indicating individually flipping a or ℓ_p reverses chirality while their joint inversion (equivalent to a $\boldsymbol{C}_2$) cannot. More specially, photonic conchs with $a \cdot \ell_p > 0$ and $a \cdot \ell_p < 0$ show opposite chiralities. The photonic conch also possesses a chiral OAM vector related to both intensity and phase distributions (see detail in Supplemental Material [33]). Instead, toroidal STOVs with $a = 0$ lack these properties.

Experimental generation of photonic conchs.—To experimentally confirm photonic conchs, we apply a strategy resembling toroidal STOV generation [Fig. 2(a)] [16]: first, STB tubes with adjustable topological charges are produced from Gaussian-like pulses via a $4f$ pulse shaper [27,42]; second, we perform inverse spiral transformation to the STB tubes, using two phase elements according to ray-optics transformation technology [28,38]. In the second process, one element transforms STB tubes into spiral-like beams via propagation of a distance of d, followed by another that collimates the fields and completes the transformation after additional d propagation.

Notably, the ideal STB vortex is experimentally unfeasible due to its infinite range along x and τ. Instead, a spatiotemporal Bessel-Gauss (STBG) vortex could be produced by introducing a Gaussian envelope $\exp\{-[x^2 + (\tau^2/\beta_0\beta_2)]/w_0^2\}$ to restrict the beam range, where w_0 is the beam waist. These STBG vortices behave similarly to STB vortices [43,44]. We generate STBG vortices with $\ell_s = 5$ and 15, using ~800 nm, ~35 fs pulses. Their spatiotemporal bandwidths are set to $\Delta k_x = \sim 61.5$ rad/mm and $\Delta\lambda = \sim 6$ nm, respectively. The parameters for coordinate transformation are $r_0 = 2$ mm, $2\pi a = 1.4$, $2\pi\beta = 15.1$ mm, and $d = 50$ mm (see detail in Supplemental Material [33]).

The spiral-like structures (in the $u - v$ plane) of photonic conchs—confirmed by the time-integrated intensities in Figs. 2(b) and 2(c)—are measured at ~50 mm distance post-transformation (see additional evidence in confirming the conch structure in Supplemental Material [33]). We rebuild the three-dimensional profiles using Mach-Zehnder scanning interferometry [45,46], with the STBG-vortex-like local field distributions [lower panels in Figs. 2(b) and 2(c)] of the anticlockwise (clockwise) photonic conch extracted at azimuthal angles $\phi = -80°, -25°, 45°$, and 105° ($\phi = 110°, 35°, -30°$, and $-90°$). In Fig. 2(a), the transformation processes also reveal an important relationship: $\ell_p = \pm\ell_s$, wherein the sign depends on the bending direction of the original STB tube (see another example in Supplemental Material [33]); therefore, the local phases in Figs. 2(b) and 2(c) show opposite phase gradient directions. Photonic conchs with a wider-angle range ($>2\pi$) could be achieved via large-size phase devices [47].

Propagation dynamics of photonic conchs in free space.—Interestingly, photonic conchs exhibit chirality-related dynamical evolution in free space, evidenced by their distinct ϕ-related states in each local field, indicating photonic conchs are solutions to FME only in anomalous

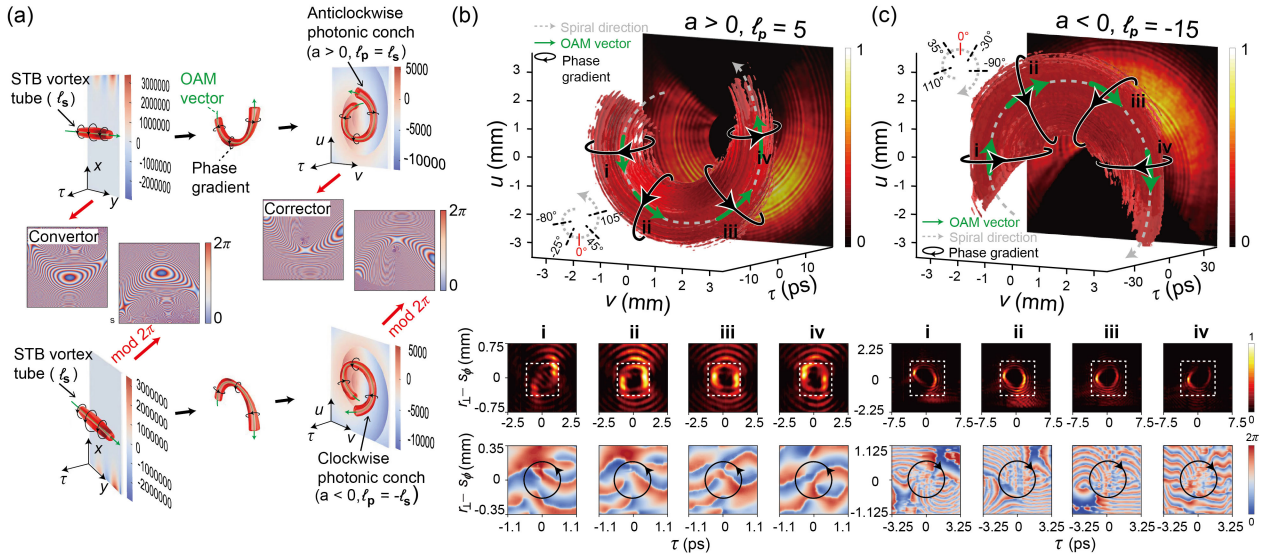

FIG. 2. (a) Photonic conch generation. (b) Three-dimensional profiles of an anticlockwise photonic conch with $\ell_p = 5$, wherein lower panels present the local intensity and phase. White dashed boxes in the intensity indicate the regions corresponding to the phase plots. (c) Similar to (b) but for a clockwise photonic conch with $\ell_p = -15$. Azimuthal angles $\phi = 0°$ in (b),(c) correspond to the points with radiuses of r_0.

dispersion. At a specific ϕ, the local field behaves like an STBG vortex, influenced by time diffraction arising from different transmission phases across its various wavelength components [18,24]. This effect can be described by a group dispersion delay model that incorporates an intrinsic dispersion factor [27] $\beta_2^{\mathrm{int}} \approx \gamma^2 c/\omega_0$, where c is the vacuum speed of light, $\gamma = \Delta k_x/\Delta\omega$ the spatiotemporal bandwidth ratio (the spatial to temporal bandwidth proportion). By solving FME, we further uncover a one-to-one correspondence between the material dispersion and the spatiotemporal bandwidth ratio of a time-diffraction-free STB vortex, i.e., $\gamma = \sqrt{-\beta_2\beta_0}$ (see detail in Supplemental Material [33]). This provides a quantitative explanation for the conventional wisdom that STOVs can exist stably under anomalous dispersion [48,49].

The chirality-related evolution can be attributed to azimuthal intrinsic dispersion. Re-examining the inverse spiral transformation reveals a slight ϕ-related change in the photonic conchs' spatial width [Fig. 3(a)], which influences spatiotemporal bandwidth ratios due to the invariance of the τ axis during transformation. This also stems from the pretransformation STBG tube having a certain spatial width rather than being a widthless line. In the first loop ($\phi \in [-\pi, \pi)$), the azimuthal intrinsic dispersion reads (see detail in Supplemental Material [33]):

$$\beta_2^{\mathrm{int}}(\phi) = \frac{x_0^2}{r_0^2 \exp(2a\phi)\exp\left(\frac{2a^2x_0}{b}\right)\sinh^2\left(\frac{x_0}{b}\right)}\beta_2^{\mathrm{int}}, \quad (5)$$

where β_2^{int} and $2x_0$ are the intrinsic dispersion and spatial width of the pretransformation STBG tube. Equation (5) also indicates toroidal STOVs with $a = 0$ exhibit azimuth-independent intrinsic dispersion. Notably, the chirality-related dynamical evolution here differs from the "dynamic chirality" describing the chiral light-matter interactions in Ref. [6].

Because of geometrical chirality, the evolution of photonic conchs with $\pm a$ satisfies mirror symmetry in the $u - v$ plane; therefore, we investigate anticlockwise photonic conchs with different topological charges. For the shift between $\ell_p = 5$ and -10, Eq. (5) reveals a slight influence (<1.05%) on the ratio $\beta_2^{\mathrm{int}}(\phi)/\beta_2^{\mathrm{int}}$ that is proportional to the evolution rate. Thus, we only present the results for $\ell_p = 5$ in Fig. 3(b). Notably, $\beta_2^{\mathrm{int}}(\phi)/\beta_2^{\mathrm{int}}$ can be effectively modulated by changing the spiral parameter. This control is intriguing for a relatively small a (e.g., $a = 0.2a_0$), as $\beta_2^{\mathrm{int}}(\phi)$ relates linearly to ϕ; but for a larger a (e.g., $a = 2a_0$), the control nearly invalids at a larger ϕ. Moreover, photonic conchs with azimuth-independent intrinsic dispersion can be achieved from spatially customized spatiotemporal tubes (see detail in Supplemental Material [33]).

As expected, the experiment shows the local fields at $\phi = -80°, 0°$, and $105°$ exhibit diverse evolutions during further propagation of 60 mm. For $\ell_p = 5$ and $\phi_0 = -80°$, the rebuilt profile shows the fastest evolution, with the field evolving quickly from an STBG vortex to a field with $\ell_p + 1$ lobes [Fig. 3(c)]. For $\phi_0 = 0°$ and $105°$, the evolution decelerates, corresponding to the decrease in $\beta_2^{\mathrm{int}}(\phi)$. Since flipping ℓ_p is equivalent to reversing τ axis, the results for $\ell_p = -10$ are similar to the τ mirror image of $\ell_p = 5$ [Fig. 3(d)]. However, all local fields maintain a vortexlike distribution without lobes, indicating higher-order photonic conchs are less sensitive to time diffraction. The difference between theoretical and experimental photonic conchs—reflected in the varying beam divergence angles [green dashed lines in Figs. 3(c) and 3(d)] at different ϕ—stems from additional diffraction introduced by ray-optics transformation and amplified by propagation in the experiment. Nevertheless, the measured divergence angles enable us to estimate $\beta_2^{\mathrm{int}}(\phi)/\beta_2^{\mathrm{int}}$ of the generated photonic conchs before propagation, yielding an acceptable agreement with the theory [Fig. 2(b), see detail in Supplemental Material [33]]. This difference might be circumvented by directly generating photonic conchs using integrated metasurfaces [39,40].

Space-time varying OAM.—Notably, the photonic conch exhibits space-time varying OAM density due to its

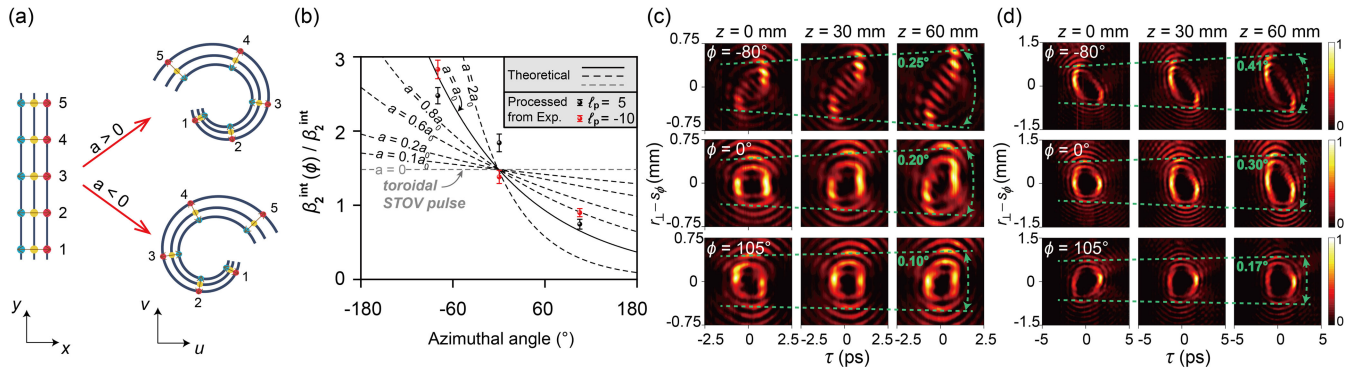

FIG. 3. (a) Principle of the azimuthal intrinsic dispersion. (b) Ratios $\beta_2^{\mathrm{int}}(\phi)/\beta_2^{\mathrm{int}}$ calculated from Eq. (5) and the processed experimental data. (c) Local field evolution for the $\ell_p = 5$ photonic conch. (d) Similar to (c) but for $\ell_p = -10$. The green dashed lines in (c),(d) mark the beam divergence angles at different ϕ. Exp.: Experiment.

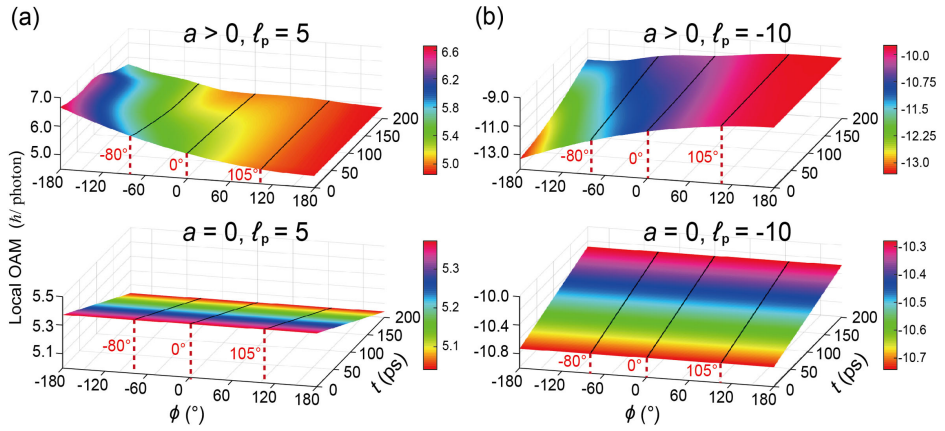

FIG. 4. (a) Calculated integral OAM value of anticlockwise photonic conch and toroidal STOV with $\ell_p = 5$ as a function of ϕ and $t = z/c$. (b) Similar to (a) but for $\ell_p = -10$.

changing integral OAM value during evolution. We extend the group dispersion delay model [27] to include the azimuthal intrinsic dispersion for describing the local field at various ϕ and z:

$$E_{\mathrm{local}}(r_\perp - s_\phi, \tau, z, \phi) \cong \int_{-\infty}^{+\infty} d(\omega-\omega_0) \int_{-\infty}^{+\infty} \tilde{E}_{\ell_p}(k_\perp, \omega-\omega_0, \phi) e^{\frac{i}{2}[\beta_2^{\mathrm{int}}(\phi)+\beta_2](\omega-\omega_0)^2 z} e^{i[k_\perp(r_\perp - s_\phi)-(\omega-\omega_0)\tau]} dk_\perp, \quad (6)$$

where $k_\perp$ and ω are the spatiotemporal frequencies of local fields at different ϕ, and $\tilde{E}_{\ell_p}$ the corresponding spatiotemporal spectrum. To characterize the phase gradient, we calculate the canonical momentum density [50], i.e., $\langle \mathbf{L} \rangle = 1/\varepsilon_0\omega_0 \int \mathbf{r} \times \mathbf{p}\, dV / (\int E^*_{\mathrm{local}} E_{\mathrm{local}} dV)$, where E_{local} can be calculated by Eq. (6), ε_0 is the dielectric constant, $\mathbf{r}$ is the position vector, and $\mathbf{p}$ is the linear momentum density related to the phase gradient. We employ the same parameters of the pretransformation STBG tubes and coordinate transformation as those used in the experiment (see corresponding local field evolutions in Supplemental Material [33]). As shown in Fig. 4, the OAM evolutions of photonic conchs with $\ell_p = 5$ and -10 map to two distinct hypersurfaces characterized by considerable local OAM gradients, varying with azimuth angle and global time $t = z/c$. Conversely, the toroidal STOVs correspond to two planes, each with relatively lower and steady OAM gradients.

Conclusion.—In summary, we demonstrate chiral-symmetry-broken toroidal wave packets, synthesize such photonic conchs with controllable topological charges, and enable the observation of previously neglected toroidal state dynamics. This also lays the framework for extending toroidal STOVs via other conformal transformations [51]. Using photonic conchs (or STOVs) for chiral light-matter interactions remains an exciting and open question. The Hamiltonian governing STOV-matter interactions might connect to the topological charge through the electric quadrupole couplings, similar to longitudinal OAM beams [52,53]. Additional complexity may arise from the inherent spin-orbital interaction within STOVs [24], while the geometrical chirality observed here could offer extra control. Encoding information into photonic conchs and selectively coupling with spiral-type antennas may enhance optical communication capacity [13,54]. Although transient, photonic conchs may transmit data over set distances and be reconstructed for long-range communication using appropriate systems [24,27]. Superposing them with longitudinal OAM might further improve communication [55]. Regulating their geometrical chirality could also facilitate the manipulation of microparticles [56]. As unique wave packets with space-time varying OAM, photonic conchs have deepened our understanding of optical OAM, likely driving progress in acoustics, electronics, and general physics.

We thank Jiang-Shan Tang, Zhao-Xian Chen, and Ling-Ling Ma for their careful reading and comments on the manuscript. The work of C. W., Y. L., A. Z. Y., H. C., W. H., and Y. Q. L. was supported by the National Key Research and Development Program of China (No. 2022YFA1405000), the Natural Science Foundation of Jiangsu Province, Major Project (No. BK20212004), the Innovation Program for Quantum Science and Technology (No. 2021ZD0301500) and the National Natural Science Foundation of China (No. 62035008 and No. 62305157). The work of W. Q. and L. S. C. was supported by the National Key Research and Development Program of

China (No. 2021YFB3600500), the National Natural Science Foundation of China (No. 61975140 and No. 62075145), and the Priority Academic Program Development of Jiangsu Higher Education Institutions.

*These authors contributed equally to this letter.
†Corresponding author: wqiao@suda.edu.cn
‡Corresponding author: lschen@suda.edu.cn
§Corresponding author: yqlu@nju.edu.cn

[1] U. Meierhenrich, *Amino Acids and the Asymmetry of Life* (Springer, Berlin, 2008).
[2] W. L. Noorduin *et al.*, Complete chiral symmetry breaking of an amino acid derivative directed by circularly polarized light, Nat. Chem. **1**, 729 (2009).
[3] M. O. Lorenzo, C. J. Baddeley, C. Muryn, and R. Raval, Extended surface chirality from supramolecular assemblies of adsorbed chiral molecules, Nature (London) **404**, 376 (2000).
[4] R. E. Gawley and J. Aubé, *Principles of Asymmetric Synthesis* (Elsevier, New York, 2012).
[5] H. Zhu, J. Yi, M.-Y. Li, J. Xiao, L. Zhang, C.-W. Yang, R. A. Kaindl, L.-J. Li, Y. Wang, and X. Zhang, Observation of chiral phonons, Science **359**, 579 (2018).
[6] Y. Tang and A. E. Cohen, Optical chirality and its interaction with matter, Phys. Rev. Lett. **104**, 163901 (2010).
[7] E. Hendry, T. Carpy, J. Johnston, M. Popland, R. V. Mikhaylovskiy, A. J. Lapthorn, S. M. Kelly, L. D. Barron, N. Gadegaard, and M. Kadodwala, Ultrasensitive detection and characterization of biomolecules using superchiral fields, Nat. Nanotechnol. **5**, 783 (2010).
[8] T. Kosaka, S. Iwai, Y. Inoue, T. Moriuchi, and T. Mori, Solvent and temperature effects on dynamics and chiroptical properties of propeller chirality and toroidal interaction of hexaarylbenzenes, J. Phys. Chem. A **122**, 7455 (2018).
[9] M. Guo *et al.*, Toroidal polar topology in strained ferroelectric polymer, Science **371**, 1050 (2021).
[10] L. Ding *et al.*, Field-tunable toroidal moment in a chiral-lattice magnet, Nat. Commun. **12**, 5339 (2021).
[11] P. G. Saffman, *Vortex Dynamics* (Cambridge University Press, Cambridge, England, 1992).
[12] A. E. Miroshnichenko, A. B. Evlyukhin, Y. F. Yu, R. M. Bakker, A. Chipouline, A. I. Kuznetsov, B. Luk'yanchuk, B. N. Chichkov, and Y. S. Kivshar, Nonradiating anapole modes in dielectric nanoparticles, Nat. Commun. **6**, 8069 (2015).
[13] N. Papasimakis, V. A. Fedotov, V. Savinov, T. A. Raybould, and N. I. Zheludev, Electromagnetic toroidal excitations in matter and free space, Nat. Mater. **15**, 263 (2016).
[14] C. Donnelly, K. L. Metlov, V. Scagnoli, M. Guizar-Sicairos, M. Holler, N. S. Bingham, J. Raabe, L. J. Heyderman, N. R. Cooper, and S. Gliga, Experimental observation of vortex rings in a bulk magnet, Nat. Phys. **17**, 316 (2021).
[15] A. Zdagkas, C. McDonnell, J. Deng, Y. Shen, G. Li, T. Ellenbogen, N. Papasimakis, and N. I. Zheludev, Observation of toroidal pulses of light, Nat. Photonics **16**, 523 (2022).
[16] C. H. Wan, Q. Cao, J. Chen, A. Chong, and Q. Zhan, Toroidal vortices of light, Nat. Photonics **16**, 519 (2022).
[17] R. W. Hellwarth and P. Nouchi, Focused one-cycle electromagnetic pulses, Phys. Rev. E **54**, 889–895 (1996).
[18] K. Y. Bliokh and F. Nori, Spatiotemporal vortex beams and angular momentum, Phys. Rev. A **86**, 033824 (2012).
[19] N. Jhajj, I. Larkin, E. W. Rosenthal, S. Zahedpour, J. K. Wahlstrand, and H. M. Milchberg, Spatiotemporal optical vortices, Phys. Rev. X **6**, 031037 (2016).
[20] S. W. Hancock, S. Zahedpour, A. Goffin, and H. M. Milchberg, Free-space propagation of spatiotemporal optical vortices, Optica **6**, 1547 (2019).
[21] A. Chong, C. Wan, J. Chen, and Q. Zhan, Generation of spatiotemporal optical vortices with controllable transverse orbital angular momentum, Nat. Photonics **14**, 350 (2020).
[22] G. Gui, N. J. Brooks, H. C. Kapteyn, M. M. Murnane, and C.-T. Liao, Second harmonic generation and the conservation of spatiotemporal orbital angular momentum of light, Nat. Photonics **15**, 608 (2021).
[23] S. W. Hancock, S. Zahedpour, and H. M. Milchberg, Second-harmonic generation of spatiotemporal optical vortices and conservation of orbital angular momentum, Optica **8**, 594 (2021).
[24] K. Y. Bliokh, Spatiotemporal vortex pulses: Angular momenta and spin-orbit interaction, Phys. Rev. Lett. **126**, 243601 (2021).
[25] S. W. Hancock, S. Zahedpour, and H. M. Milchberg, Mode structure and orbital angular momentum of spatiotemporal optical vortex pulses, Phys. Rev. Lett. **127**, 193901 (2021).
[26] Y. Fang, S. Lu, and Y. Liu, Controlling photon transverse orbital angular momentum in high harmonic generation, Phys. Rev. Lett. **127**, 273901 (2021).
[27] W. Chen, W. Zhang, Y. Liu, F. C. Meng, J. M. Dudley, and Y. Q. Lu, Time diffraction-free transverse orbital angular momentum beams, Nat. Commun. **13**, 1 (2022).
[28] Y. Wen, I. Chremmos, Y. Chen, J. Zhu, Y. Zhang, and S. Yu, Spiral transformation for high-resolution and efficient sorting of optical vortex modes, Phys. Rev. Lett. **120**, 193904 (2018).
[29] A. V. Husakou and J. Herrmann, Supercontinuum generation of higher-order solitons by fission in photonic crystal fibers, Phys. Rev. Lett. **87**, 203901 (2001).
[30] A. Couairon, E. Brambilla, T. Corti, D. Majus, O. de J. Ramírez-Góngora, and M. Kolesik, Practitioner's guide to laser pulse propagation models and simulations, Eur. Phys. J. Special Topics **199**, 5 (2011).
[31] O. V. Borovkova, Y. V. Kartashov, V. E. Lobanov, V. A. Vysloukh, and L. Torner, General quasi-nonspreading linear three-dimensional wave packets, Opt. Lett. **36**, 2176 (2011).
[32] G. C. Berkhout, M. P. Lavery, J. Courtial, M. W. Beijersbergen, and M. J. Padgett, Efficient sorting of orbital angular momentum states of light, Phys. Rev. Lett. **105**, 153601 (2010).
[33] See Supplemental Material at http://link.aps.org/supplemental/10.1103/PhysRevLett.132.153801 for details regarding the analytical derivation, symmetry analysis, additional conch structure confirmation, and azimuthal-related and independent intrinsic dispersion of the photonic conch, which includes Refs. [16,24,27–29,32,34–40]. These files also contain experimental details, an extra example of the sign rule for the topological charge, a comparison

between experimental and theoretical photonic conchs, and the theoretical evolution of photonic conchs.

[34] G. P. Agrawal, *Nonlinear Fiber Optics* (Academic, San Diego, 2001).

[35] A. Vasara, J. Turunen, and A. T. Friberg, Realization of general nondiffracting beams with computer-generated holograms, J. Opt. Soc. Am. A **6**, 1748 (1989).

[36] E. T. Whittaker, On the partial differential equations of mathematical physics, Math. Ann. **57**, 333 (1903).

[37] A. V. Oppenheim, G. V. Frisk, and D. R. Martinez, Computation of the Hankel transform using projections. J. Acoust. Soc. Am. **68**, 523 (1980).

[38] W. J. Hossack, A. M. Darling, and A. Dahdouh, Coordinate transformations with multiple computer-generated optical elements, J. Mod. Opt. **34**, 1235 (1987).

[39] H. Wang, C. Guo, W. Jin, A. Y. Song, and S. Fan, Engineering arbitrarily oriented spatiotemporal optical vortices using transmission nodal lines, Optica **8**, 966 (2021).

[40] C. Guo, M. Xiao, M. Orenstein, and S. Fan, Structured 3D linear space–time light bullets by nonlocal nanophotonics, Light Sci. Appl. **10**, 160 (2021).

[41] A. Forbes, M. de Oliveira, and M. R. Dennis, Structured light, Nat. Photonics **15**, 253 (2021).

[42] A. M. Weiner, Femtosecond pulse shaping using spatial light modulators, Rev. Sci. Instrum. **71**, 1929 (2000).

[43] F. Gori, G. Guattari, and C. Padovani, Bessel-gauss beams, Opt. Commun. **64**, 491 (1987).

[44] M. Dallaire, N. McCarthy, and M. Piché, Spatiotemporal bessel beams: Theory and experiments, Opt. Express **17**, 18148 (2009).

[45] Y. Li and J. W. Lewellen, Generating a quasiellipsoidal electron beam by 3D laser-pulse shaping, Phys. Rev. Lett. **100**, 074801 (2008).

[46] H. Li, I. V. Bazarov, B. M. Dunham, and F. W. Wise, Three-dimensional laser pulse intensity diagnostic for photoinjectors, Phys. Rev. ST Accel. Beams **14**, 112802 (2011).

[47] F. Zhou, F. Zhou, Y. Chen, J. Hua, W. Qiao, and L. Chen, Vector light field display based on an intertwined flat lens with large depth of focus, Optica **9**, 288 (2022).

[48] C. Wan, A. Chong, and Q. Zhan, Optical spatiotemporal vortices, eLight **3**, 11 (2023).

[49] Q. Cao, Z. Chen, C. Zhang, A. Chong, and Q. Zhan, Propagation of transverse photonic orbital angular momentum through few-mode fiber, Adv. Photonics **5**, 036002 (2023).

[50] L. Allen, M. W. Beijersbergen, R. J. C. Spreeuw, and J. P. Woerdman, Orbital angular momentum of light and the transformation of Laguerre-Gaussian laser modes, Phys. Rev. A **45**, 8185 (1992).

[51] J. W. Brown and R. V. Churchill, *Complex Variables and Applications* (McGraw-Hill, New York, 2009).

[52] K. A. Forbes and D. L. Andrews, Optical orbital angular momentum: Twisted light and chirality. Opt. Lett. **43**, 435 (2018).

[53] K. A. Forbes and D. L. J. Andrews, Orbital angular momentum of twisted light: Chirality and optical activity, J. Phys. Photonics **3**, 022007 (2021).

[54] F. Cardano and L. Marrucci, Smoke rings of light, Nat. Photonics **16**, 476 (2022).

[55] C. Wan, J. Chen, A. Chong, and Q. Zhan, Photonic orbital angular momentum with controllable orientation, Natl. Sci. Rev. **9**, nwab149 (2021).

[56] A. B. Stilgoe, T. A. Nieminen, and H. Rubinsztein-Dunlop, Controlled transfer of transverse orbital angular momentum to optically trapped birefringent microparticles, Nat. Photonics **16**, 346 (2022).